Origins of the damping in perpendicular media: Three component ferromagnetic resonance linewidth in Co–Cr–Pt alloy films

Nan Mo,[1,a)] Julius Hohlfeld,[2] Misbah ul Islam,[1,5] C. Scott Brown,[1] Erol Girt,[3] Pavol Krivosik,[1,4] Wei Tong,[1] Adnan Rebei,[2] and Carl E. Patton[1,2]
[1]*Department of Physics, Colorado State University, Fort Collins, Colorado 80523, USA*
[2]*Seagate Research, Pittsburgh, Pennsylvania 15222, USA*
[3]*Seagate Technology, Fremont, California 94538, USA*
[4]*Slovak University of Technology, 81219 Bratislava, Slovak Republic*
[5]*Department of Physics, Bahauddin Zakariya University, Multan, Pakistan*

(Received 12 November 2007; accepted 21 December 2007; published online 15 January 2008)

The 9.41 GHz ferromagnetic resonance field and linewidth have been measured as a function of the angle (θ_H) between the external magnetic field and film normal for a series of 17.5 nm thick Co–Cr–Pt alloy films. The linewidths ranged from hundreds of Oersted to kiloersted, with different values at $\theta_H=0$ and $\theta_H=90°$ and additional minima and maxima for θ_H-values from 16° to 64°. The profiles can be fitted with a combination of inhomogeneity line broadening, grain boundary two magnon scattering, and magnon-electron (*m-e*) scattering processes, with a notably small Gilbert damping α-value of 0.004 for the *m-e* term. © *2008 American Institute of Physics*.
[DOI: 10.1063/1.2834835]

Perpendicular recording[1] provides one way to achieve the next generation of high density storage in the range of terabits/inch^2. Co–Cr–Pt thin films, with perpendicular anisotropy and nanometer sized grains,[2] represent one material of choice for such systems. In addition to anisotropy and microstructure, the damping or relaxation plays an essential role in recording. Up to now, cited damping values are usually based on a Gilbert or nominally equivalent Landau-Lifshitz phenomenological formulation. Fits to data generally require much larger Gilbert damping parameters than found for the usual low loss ferromagnetic metal films. These phenomenological models, moreover, do not take into account any physical relaxation process.

This letter presents ferromagnetic resonance (FMR) results on a series of Co–Cr–Pt alloy films that clarify and quantify the physical damping processes for perpendicular media materials. The data show that the FMR linewidth is (1) quite large and (2) a somewhat complicated function of the static magnetic field orientation. There are two dominant linewidth contributions, inhomogeneity line broadening (ILB)[3] and two magnon grain boundary scattering (GBS),[4] that cannot be described through phenomenological models alone. The Gilbert contribution, and the corresponding specific physical process of magnon electron (*m-e*) scattering that can be rigorously connected to this phenomenological model,[5] comprise a very small part of the overall linewidth.

The measurements were made on four 17.5 nm thick, 9 mm diameter films of different compositions, all sputter deposited on glass substrates. Table I lists film properties. Vector vibrating sample magnetometry (VVSM) was used to determine the saturation magnetic induction $4\pi M_s$. The effective induction, $B_{s\text{-eff}}=4\pi M_s-H_u$, where H_u is an effective perpendicular uniaxial anisotropy field, and the gyromagnetic ratio γ were obtained from the FMR field versus field angle data. The corresponding H_u values are shown in the last column of Table I. These are within 10% of the H_u values obtained from the VVSM data. These films have a relatively weak anisotropy and $B_{s\text{-eff}}>0$. These particular samples were chosen to allow for x-band FMR measurements with the available maximum field of 12 kOe.

The FMR measurements were made with a reflection cavity microwave spectrometer at a frequency $\omega/2\pi=9.41$ GHz. Field modulation and lock-in techniques were used to obtain the field derivative of the FMR absorption profile, taken here as $D(H_{\text{ext}})$, where H_{ext} denotes the static external field. The FMR field H_{FMR} and the derivative linewidth were obtained as the average and difference, respectively, of the fields at the peak and dip of the $D(H_{\text{ext}})$ profile. Based on the working assumption of a Lorentzian line shape, the derivative linewidth multiplied by $\sqrt{3}$ yields the standard half power linewidth ΔH. Determinations of H_{FMR} and ΔH were obtained from $D(H_{\text{ext}})$ measurements as a function of the angle θ_H between $\mathbf{H}_{\text{ext}}$ and the film normal.

Figure 1 shows representative results on the $H_{\text{FMR}}(\theta_H)$ and $\Delta H(\theta_H)$. These particular data and fits are for sample C. The open circles show the data. The curves show theoretical fits. The curve in (a) is based on standard FMR theory for a uniformly magnetized film with the vector magnetization $\mathbf{M}_s$ in static equilibrium at some angle $\theta_M(H_{\text{ext}}, B_{s\text{-eff}}, \theta_H)$ that follows the usual Stoner-Wohlfarth model for thin films with a perpendicular-to-plane uniaxial anisotropy. The data and the theory match nicely. Similar results were obtained for all samples.

The linewidth data and the theoretical curves in Fig. 1(b) provide proof positive that the FMR losses in these

TABLE I. Material parameters for the Co–Cr–Pt film samples.

Label	Pt (at. %)	Cr (at. %)	$4\pi M_s$ (G)	$B_{s\text{-eff}}$ (G)	$\lvert\gamma\rvert/2\pi$ (MHz/G)	H_u (Oe)
A	0	10	12549	6357	2.89	6192
B	0	15	11106	3469	2.96	7637
C	8	5	14126	2851	3.16	11275
D	8	10	11872	6	3.77	11871

[a)]Electronic mail: monan@lamar.colostate.edu.

 © 2008 American Institute of Physics
Downloaded 24 Jan 2008 to 129.82.140.224. Redistribution subject to AIP license or copyright; see http://apl.aip.org/apl/copyright.jsp

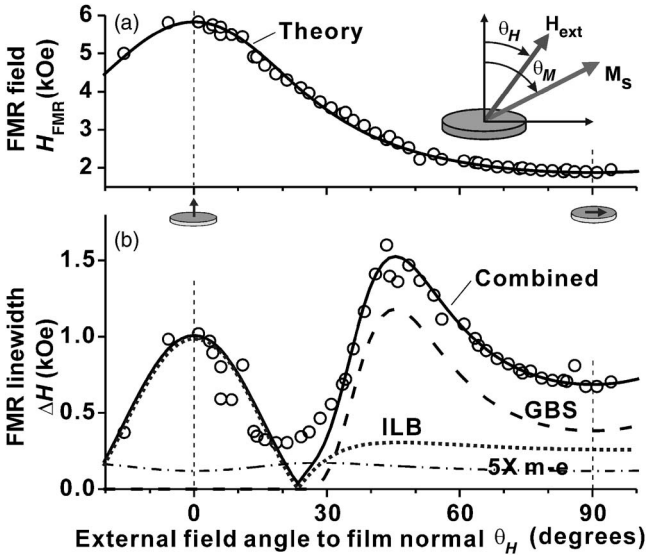

FIG. 1. Graphs (a) and (b) show results on the 9.41 GHz ferromagnetic resonance (FMR) field H_{FMR} and half power linewidth ΔH as a function of the angle θ_H between the static external field $\mathbf{H}_{ext}$ and film normal, respectively, for sample C. The inset shows the sample field ($\mathbf{H}_{ext}$), magnetization ($\mathbf{M}_s$), and angle geometry. θ_M is the angle between $\mathbf{M}_s$ and the film normal. The open circles show the data and the solid curves show computed results. The dotted, dashed, and dot-dashed curves in (b) show the computed linewidth components for inhomogeneity line broadening (ILB), two magnon grain boundary scattering (GBS), and magnon electron (*m-e*) scattering, respectively. The *m-e* curve is shown in ×5 magnification.

Co–Cr–Pt films are dominated by the ILB and GBS processes, with only a small part due to Gilbert consistent (*m-e*) scattering intrinsic losses. These three linewidth terms and the fits are discussed below. See Ref. 6 for an up-to-date review of damping and relaxation processes in metallic magnetic films. Overall, the 0.25–1.5 kOe linewidths are quite large compared to intrinsic metallic film x-band linewidths that typically fall in the 30–50 Oe range.[7] One of the key results evident for sample C is that the overall $\Delta H(\theta_H)$ response, with distinct peaks at $\theta_H=0$ and $\theta_H\approx 45°$, a prominent dip at $\theta_H\approx 20°$, and unequal linewidths at θ_H values of zero and 90°, is nothing like the profile expected from an LL or Gilbert linewidth model. A pure Gilbert damping based ΔH versus θ_H profile would look like the *m-e* curve in Fig. 1(b), but scaled up to fit the substantially larger measured linewidths. For such an exercise, the rough Gilbert damping parameter α for the scaling would be in the range of 0.1, but the shape of the $\Delta H(\theta_H)$ response would be all wrong. Many workers tout large α-values for perpendicular media thin films. The present results show that such a treatment is, at best, problematic.

Now consider the ILB, GBS, and *m-e* processes one by one. The ILB process comes from the superposition of many local FMR profiles for different regions of the sample that are shifted in field because of some magnetic property change.[8] The ILB effect on the FMR linewidth in metallic films is well established. References 3 and 9 present consistent analyses based on a region-to-region variation in $B_{s\text{-eff}}$. The ILB linewidth is given by $\Delta H_{ILB}\approx|\partial H_{FMR}/\partial B_{s\text{-eff}}|\times\Delta B_{s\text{-eff}}$, where $\Delta B_{s\text{-eff}}$ denotes the width of the distribution in local $B_{s\text{-eff}}$ values over the film. The size of the response is controlled by the spread in $B_{s\text{-eff}}$ values expressed through $\Delta B_{s\text{-eff}}$. The corresponding computation with an angle independent $\Delta B_{s\text{-eff}}$ value of 985 G leads to the ILB curve in Fig. 1(b). The sharp cusp and the $\Delta H_{ILB}=0$ point at $\theta_H\approx 23°$ correspond to the case that the FMR field does not depend on $B_{s\text{-eff}}$ to lowest order. The largest ΔH_{ILB} value at $\theta_H=0$ corresponds to the case that H_{FMR} changes linearly with $B_{s\text{-eff}}$ and ΔH_{ILB} is most sensitive to any $B_{s\text{-eff}}$ variation. At $\theta_H=90°$, the FMR frequency scales with the square root of the FMR field and the ILB effect is reduced.

Inhomogeneities are also the basis for two magnon scattering processes,[10] a well established contributor to FMR linewidths. Briefly stated, local inhomogeneities such as a nonuniform grain-to-grain anisotropy, pores, grain boundaries, etc., can break the orthogonality between the driven FMR mode and other degenerate spin wave modes. The two magnon linewidth comes from the coupling and energy transfer between these modes. For grain-to-grain inhomogeneities, the coupling is large for spin waves with a wave number (k) close to zero and then drops rapidly to zero as k increases. The decay length in k is on the order of $1/a_0$, where a_0 denotes the average grain diameter.

The present data, however, indicate that grain boundary scattering rather than grain scattering is the dominant two magnon effect in these nanometer grain sized films. Quite fortuitously, a two magnon GBS theory has been developed recently for bulk polycrystalline ferrites with micron sized grains.[4] With suitable modifications for the thin film spin wave dispersion, the GBS relaxation rate η_{GBS} for thin films can be obtained directly from this theory. Several specific modifications are needed. It is assumed that (1) the participant modes are uniform over the film cross section, (2) the spin wave wave vectors ($\mathbf{k}$) lie in the film plane, and (3) the Harte spin wave dispersion equations for thin films apply.[11,12] One also assumes that the grain boundaries are columnar and aligned with the film normal. Finally, it is assumed that the grain size (a) follows a Gaussian distribution centered at $a=a_0$ and with a standard deviation σ_a.

The GBS two magnon theory yields a thin film relaxation rate of the form

$$\eta_{GBS}=C\Lambda(\theta_H)\int_0^{k_{max}}\left[\frac{\pi^2k^2a_0^2g(ka_0,1,\sigma_a/a_0)}{(1+k^2a_0^2)^{3/2}}\right]\rho_k(k,\theta_H)dk. \quad (1)$$

Here, C is equal to $3\gamma^2K_s^2/M_s^2$, where K_s is a surface anisotropy energy density parameter, $\Lambda(\theta_H)$ is a mode polarization factor that is on the order of unity, and k_{max} is the cutoff wave number for degenerate spin waves. The square bracket term corresponds to the Fourier transform of the self-correlation function for the surface anisotropy fields at the grain boundaries. The g function denotes a standard normalized Gaussian distribution for a variable ka_0 with a mean value of unity and a standard deviation σ_a/a_0. The ρ_k corresponds to the spin wave density of degenerate states (DOS) per unit k. Once computed, this η_{GBS} may be converted to the usual field swept field linewidth in the standard way.[7]

Figure 2 demonstrates the role of the different factors in Eq. (1) on the GBS relaxation rate. The top part shows spin wave band diagrams of spin wave frequency ω_k versus k for different θ_H values, as indicated. The top and bottom boundaries of the shaded bands correspond to in-plane $\mathbf{k}$ vectors that are perpendicular and parallel to the direction of the in-plane projection of $\mathbf{M}_s$. The diagrams are shown for a common $k=0$ FMR frequency point. The solid and dashed

Downloaded 24 Jan 2008 to 129.82.140.224. Redistribution subject to AIP license or copyright; see http://apl.aip.org/apl/copyright.jsp

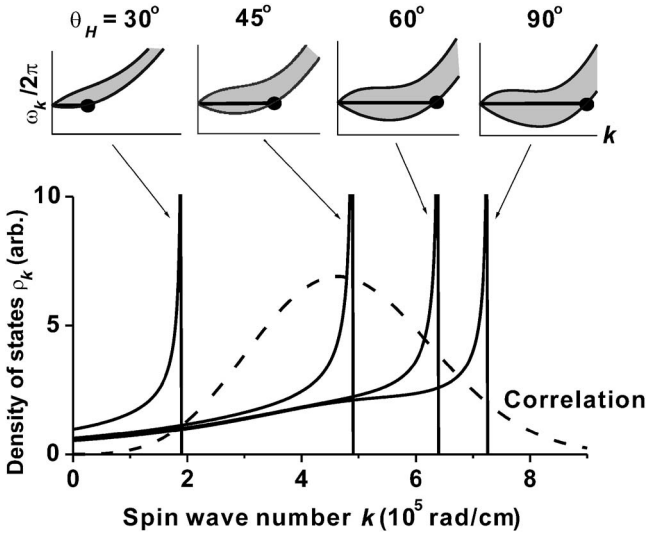

FIG. 2. The top diagrams show the change in the spin wave dispersion band of frequency ω_k vs wave number k with field angle θ_H, with the FMR frequency at $k=0$ held constant. The horizontal lines and dots mark the k-values for the degenerate modes. The graph shows the corresponding curves for the density of states ρ_k for the degenerate spin waves (solid curves), as well as the Fourier transform of the self correlation between k and the grain boundary surface anisotropy fields (dashed curve), as a function of k, based on the parameters for sample C, along with an exchange stiffness parameter value of 6×10^{-9} cm^2 Oe/rad^2.

curves in the bottom graph show, respectively, the density of states function ρ_k and the square bracket self-correlation term from Eq. (1) as a function of k.

One can see from Fig. 2 that there is a DOS peak at $k=k_{\max}$ and that this peak shifts up in k as the θ_H increases. This shifting DOS peak then moves through the broad maximum in the self correlation profile just at $\theta_H\approx45°$. This is the basic origin of the peak in the GBS linewidth at this angle, as evident from the sample C data. Note that for $\theta_H<23°$ or so, there are no degenerate $k\neq0$ spin waves and the GBS relaxation rate is zero. This is the reason for the cutoff in the GBS linewidth in Fig. 1 for θ_H values below about 27°.

The final process to consider is *m-e* scattering, expressed in terms of a Gilbert damping parameter α. The *m-e* curve in Fig. 1(b) shows the computed θ_H-dependent linewidth obtained with $\alpha=0.004$. This α value is in the same range as the usual intrinsic damping found in other transition metal films. The main point for this work is that for the present films and the large overall linewidths, one can obtain a consistent and physically sound picture of the damping through the combination of relatively large ILB and GBS contributions to ΔH, along with a relatively small and materials consistent *m-e* linewidth. Overall, the *m-e* scattering term and the corresponding α value amount to only a small background intrinsic contribution to the damping.

TABLE II. Ferromagnetic resonance linewidth fit parameters.

Sample	$\Delta B_{s\text{-eff}}$ (G)	a_0 (nm)	K_s (erg/cm^2)	σ_a/a_0	α
A	300	36	0.07	0.415	0.004
B	406	31	0.07	0.50	0.004
C	985	23	0.14	0.415	0.004
D	1330	26	0.19	0.48	0.004

The results for the other samples follow the same pattern, with relatively large ILB and GBS contributions and a small *m-e* contribution to the linewidth, along with consistent fits to the $\Delta H(\theta_H)$ data. The GBS peaks for samples A, B, and D are at $\theta_H\approx16°$, 43°, and 64°, respectively. The parameter values for the overall fits for all samples are given in Table II. These fits were done for the same Gilbert damping value (0.004) and exchange stiffness value (6×10^{-9} cm^2 Oe/rad^2). It is noteworthy that the fitted K_s values for the four samples are in the expected range for Co–Pt films.[13]

This work was supported in part by the U. S. Army Research Office, MURI Grant No. W911NF-04-1-0247, the Office of Naval Research (USA), Grant No. N00014-06-1-0889, the Information Storage Industry Consortium (INSIC) extremely high density recording program, and the Pakistan Higher Education Commission.

[1] S. N. Piramanayagam, J. Appl. Phys. **102**, 011301 (2007).
[2] T. Oikawa, M. Nakamura, H. Uwazumi, T. Shimatsu, H. Muraoka, and Y. Nakamura, IEEE Trans. Magn. **38**, 1976 (2002).
[3] S. T. Purcell, H. W. Van Kesteren, E. C. Cosman, W. B. Zeper, and W. Hoving, J. Appl. Phys. **69**, 5640 (1991).
[4] N. Mo, J. J. Green, P. Krivosik, and C. E. Patton, J. Appl. Phys. **101**, 023914 (2007).
[5] V. Kambersky and C. E. Patton, Phys. Rev. B **11**, 2668 (1975); L. Berger, J. Phys. Chem. Solids **38**, 1321 (1977).
[6] J. A. C. Bland and B. Heinrich, *Ultrathin Magnetic Structures III* (Springer, Berlin, 2005), p. 143.
[7] P. Krivosik, N. Mo, S. Kalarickal, and C. E. Patton, J. Appl. Phys. **101**, 083901 (2007).
[8] R. D. McMichael, D. J. Twisselmann, and A. Kunz, Phys. Rev. Lett. **90**, 227601 (2003).
[9] R. D. McMichael, J. Appl. Phys. **95**, 7001 (2004).
[10] M. Sparks, *Ferromagnetic-Relaxation Theory* (McGraw-Hill, New York, 1964).
[11] K. J. Harte, J. Appl. Phys. **39**, 1503 (1968).
[12] R. D. McMichael and P. Krivosik, IEEE Trans. Magn. **40**, 2 (2002).
[13] J. H. Kim and S. C. Shin, J. Appl. Phys. **80**, 3121 (1996).

Downloaded 24 Jan 2008 to 129.82.140.224. Redistribution subject to AIP license or copyright; see http://apl.aip.org/apl/copyright.jsp